Heat−Transfer Analogy for Wax Deposition from Paraffinic Mixtures

ARTICLE *in* INDUSTRIAL & ENGINEERING CHEMISTRY RESEARCH · DECEMBER 2003

Impact Factor: 2.59 · DOI: 10.1021/ie030573v

2 AUTHORS, INCLUDING:

Anil K Mehrotra
The University of Calgary
160 PUBLICATIONS **2,348** CITATIONS

SEE PROFILE

Article

Heat-Transfer Analogy for Wax Deposition from Paraffinic Mixtures

Hamid O. Bidmus, and Anil K. Mehrotra

Ind. Eng. Chem. Res., **2004**, 43 (3), 791-803• DOI: 10.1021/ie030573v • Publication Date (Web): 30 December 2003

Heat-Transfer Analogy for Wax Deposition from Paraffinic Mixtures

Hamid O. Bidmus and Anil K. Mehrotra*

Department of Chemical and Petroleum Engineering, University of Calgary, Calgary, Alberta, Canada T2N 1N4

Wax deposition from mixtures of a paraffinic wax (C_{20}−C_{40}) dissolved in *n*-dodecane (C_{12}) was investigated. A novel batch apparatus was developed, in which the flow of a "hot" wax−C_{12} mixture was accomplished with an axial flow propeller while the solid deposition took place on the inner "cold" surface of a draft tube. The effects of mixture composition, shear rate, residence time, and temperature on solid deposition were studied at pseudo-steady state. Predictions from a steady-state heat-transfer model were in good agreement with experimental data, which confirmed the wax deposition process to be controlled primarily by heat transfer. A temperature difference ratio corresponding to the fractional temperature difference across the deposit layer was related to the amount of deposited solids. GC analyses of the deposited solids were used to study compositional changes within the liquid and solid phases.

Introduction

The adverse effects of wax deposition are encountered in all sectors of the petroleum industry, ranging from damage to oil reservoir formations to blockage of pipelines and process equipment. The resulting decrease in the oil flow rate affects the efficiency of the processes involved and causes substantial expenditures for the control and remediation of wax deposition.

"Waxy" or paraffinic crude oils are complex mixtures that contain, among other compounds, high-molecular-weight hydrocarbons. These paraffins or waxes have a reduced solubility in crude oil at low temperatures, so that they tend to crystallize and deposit on cooler surfaces. The highest temperature at which the first crystals of paraffin wax start to appear upon cooling of a waxy crude oil is known as the wax appearance temperature (WAT). Wax particles start to crystallize out when the crude oil temperature falls below the WAT, which leads eventually to solid deposition on the pipe wall. Azevedo et al.[1] presented a review of possible wax deposition mechanisms, which include molecular diffusion, shear dispersion, Brownian movement, and gravity settling.

Holder and Winkler[2] observed paraffin wax deposits under a cross-polarized microscope and found that the wax crystallites have structures of platelets that overlap and interlock. A solid network structure is formed when sufficient quantities of solid paraffin crystals are formed, with entrapped liquid oil, leading to the formation of a gel-like structure. Thus, the wax deposit is not entirely solid but rather consists of two phases: liquid and solid. The wax−oil gelation is due to the flocculation of orthorhombic wax crystallites that appear in the solution during cooling.[3] Other studies have shown that as little as 2% of precipitated wax can be sufficient to form a gel.[4,5]

Experimental investigations have shown that wax deposits obtained at higher flow rates are considerably harder than those formed at lower flow rates.[5−10] The composition of deposited solids has been found to change somewhat with time under certain operating conditions.[5,8] The hardening and compositional changes that occur within the deposit with time lead to its "aging". Singh et al.[6] observed that paraffin molecules below a "critical carbon number" tend to diffuse out of the deposit while those with carbon number above the critical value tend to diffuse into the deposit through a counterdiffusion process. They observed that this aging process depended on operating conditions and that it was a stronger function of the temperature difference across the deposit than the compressive force due to flow. Creek et al.[8] used the phenomenon of Ostwald ripening (i.e., self-organization of wax molecules based on their area-to-size ratio) to explain the mechanism of aging.

Several factors are responsible for the formation of wax deposits in pipelines, including crude oil composition, temperature and thermal history, shear rate and shear history, and pressure. The amount of wax deposited is also affected by the concentration of paraffins, light ends, and nucleating/inhibiting materials in the crude oil.[11−15] Pressure is not regarded as an important factor for wax deposition, especially for dead or stock tank oils (STOs). Brown et al.[11] estimated that the WAT of a dead oil increases by about 2.2 °C for a 10 MPa increase in pressure, whereas Meray et al.[13] reported an increase of 3.0 °C for the same pressure increase. Other studies have shown a decrease in the amount of wax deposited with increasing flow rate.[5,8,10,16−18] The shear history, together with the thermal history, of the crude oil is also considered to be an important factor.[19,20] The difference between the bulk oil temperature and the temperature of pipe wall or the outside environment has been suggested as the driving force needed for wax deposition to occur.[8,10,21] Others have considered the difference between the WAT and the wall temperature to be important for wax deposition.[7,16,22]

Bott[23] provided relationships between the thickness of wax deposit layer, temperatures, heat-transfer coefficients and the deposit thermal resistance. Correlations for the amount of wax deposited have been developed by relating the flow rate and the oil and wall temperatures on the basis of the data acquired from experiments on waxy crude oils.[21,24] However, serious limita-

* To whom correspondence should be addressed. Tel.: (403) 220-7406. Fax: (403) 284-4852. E-mail: mehrotra@ucalgary.ca.

10.1021/ie030573v CCC: $27.50
Published on Web 12/30/2003

tions were pointed out for interpolating or extrapolating such correlations obtained by curve fitting experimental data on wax deposition.[25] By neglecting the thermal resistances due to the pipe wall and coolant flow in the wax deposition results reported by Agrawal et al.,[21] the following relationship was developed from a heat-transfer approach[26]

$$\frac{hx_d}{k_d} = \frac{2x_d}{D - 2x_d}\left(\ln\frac{D}{D - 2x_d}\right)^{-1}\frac{(T_h - T_c)}{(T_h - T_d)} \qquad (1)$$

where T_h, T_d, and T_c are the temperatures of the crude oil, the oil−deposit interface, and the coolant, respectively; h is the heat-transfer coefficient; k_d is the thermal conductivity of the deposit; D is the tube diameter; and x_d is the deposit layer thickness.

There is a decrease in the rate at which the deposit layer accumulates with time, which has been attributed to the insulation effect of the already deposited wax.[16] Ghedamu et al.[27] reported experimental measurements for solid deposition from wax−kerosene mixtures at varying wax concentrations, bulk temperatures, flow velocities, and types of deposition surface. The deposit thermal resistance was found to increase with time and reach an asymptotic value. The amount of wax deposited during the transportation of crude oils has been shown to decrease for insulated pipes, decreasing temperature differentials, and increased shear rates.[8,10,14,21,22,27,28]

It was recognized that, to gain an improved understanding of solids deposition from waxy crude oils, it would be desirable to examine simpler and more well-defined systems initially. Once sufficient understanding and data became available, a transition could be made to the more complex mixtures, i.e., waxy crude oils. Accordingly, a model system comprising a paraffinic wax as the solute and *n*-dodecane (C_{12}) as the solvent was developed to simulate waxy crude oils for laboratory investigations. Some of the advantages of working with prepared mixtures are as follows: (i) the composition of the model system remains constant during the course of experiments, in contrast to the case of working with crude oil samples where the lighter ends can be lost at higher temperatures; (ii) experiments can be performed with different compositions, which is not convenient to do for crude oils without introducing additional uncertainties; and (iii) chemical analysis and characterization of the prepared mixtures is easier and is reproducible.

This investigation was undertaken to provide an improved understanding of the wax deposition process at pseudo-steady state. The main objective of this study was to determine whether the wax deposition process could be explained by a heat-transfer analogy. It involved the development of a steady-state heat-transfer model for solid deposition from wax−solvent mixtures. An experimental methodology was developed for investigating the effects of several variables in a bench-scale apparatus. Although the scale of experimental apparatus was much smaller than that of field operations, it was considered adequate for establishing the wax deposition process to be governed by heat transfer. The experimental results obtained from extensive laboratory measurements were used to validate predictions from the heat-transfer model.

Development of the Heat-Transfer Model

During the flow of waxy crude oils through a pipeline, heat transfer to the surrounding "colder" environment

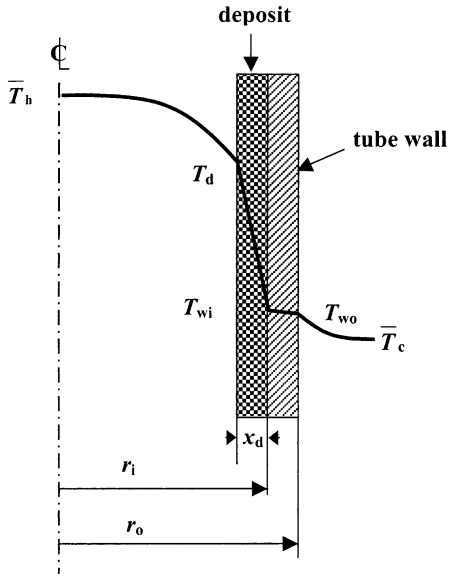

Figure 1. Temperature profile and thermal resistances involved in wax deposition.

decreases the crude oil temperature, leading to the precipitation and deposition of paraffin solids on the pipe wall. Wax crystals form a solid deposit layer involving a network of a solid (wax) phase with liquid oil trapped within it. With time, the deposit layer grows in thickness until a point is reached when growth stops.[7] At this point, the rates of heat transfer across the flowing oil, the wax deposit layer, and the pipe wall are the same and remain constant with time. Although the thickness of the deposit as well as the oil and wall temperatures attain constant values, the composition of the deposit layer has been observed to change slowly with time.[5] Nevertheless, once the deposit layer achieves a nearly constant layer thickness, the rate of heat transfer can be assumed to be under a thermal pseudo-steady state because of the relatively stable temperatures.

As shown schematically with temperature profiles in Figure 1, the transfer of thermal energy from the "hot" stream to the "cold" stream involves four thermal resistances in series: two convective resistances due to the hot and cold liquid streams and two conductive resistances due to the tube wall and the deposited solid layer. Assuming one-dimensional heat transfer in the radial direction of a tube used for heat exchange, the rate of heat transfer is equated to the rate of thermal energy lost by the hot wax−solvent mixture (simulating a waxy crude oil), the rate of thermal energy gained by the coolant, and the rate of heat exchange between hot and cold streams, as follows

$$q = \dot{m}_h C_h (T_{h-in} - T_{h-out}) = \dot{m}_c C_c (T_{c-out} - T_{c-in}) = U_i A_i (\bar{T}_h - \bar{T}_c) \qquad (2)$$

where q is the rate of heat transfer; $\dot{m}_h$ and $\dot{m}_c$ are mass flow rates of the hot and cold streams, respectively; C_h and C_c are the average specific heat capacities of the hot and cold streams, respectively; T_{h-in} and T_{h-out} are the inlet and outlet hot-stream temperatures, respectively; T_{c-out} and T_{c-in} are the outlet and inlet temperatures, respectively, of the coolant; U_i *is* the inside overall heat-transfer coefficient; A_i is the inside tube area for heat transfer; and $\bar{T}_h$ and $\bar{T}_c$ are the average hot- and cold-stream temperatures, respectively.

At steady state, the heat reflux through each of the four thermal resistances included in U_i is as follows

$$\frac{q}{A_i} = \frac{h_h(\bar{T}_h - T_d)}{r_i/(r_i - x_d)} = \frac{k_d(T_d - T_{wi})}{r_i \ln(r_i/(r_i - x_d))} = \frac{k_m(T_{wi} - T_{wo})}{r_i \ln(r_o/r_i)} = \frac{h_c(T_{wo} - \bar{T}_c)}{r_i/r_o} \quad (3)$$

where x_d is the deposit thickness (assumed to be uniform along the short tube length); T_{wi} and T_{wo} are the average inside and outside tube-wall temperatures, respectively; T_d is the temperature at the interface of the deposit layer and hot stream; h_h and h_c are the individual convective heat-transfer coefficients for the hot and cold streams, respectively; and k_d and k_m are the thermal conductivities of the deposit layer and the tube wall, respectively. Note that wax deposition calculations with eq 3 are sensitive to the values of k_d and T_d. For predictive calculations involving eq 3, the values of k_d used were 0.23, 0.27, and 0.30 W/m·K for 10, 15, and 20 mass % wax−C_{12} mixtures, respectively. For the solidification or melting of a pure substance, the liquid−deposit interface temperature, T_d, is the melting or freezing temperature, but it is the liquidus temperature for a multicomponent mixture. From a modeling study, Singh et al.[5] estimated T_d to approach the WAT when the deposit layer thickness stops growing. As discussed later, experimental verification of T_d and the WAT being the same temperature is an important contribution of this study.

The overall thermal resistance is expressed as the sum of four individual thermal resistances, as follows[26]

$$\frac{1}{U_i A_i} = \frac{1}{h_h A_h} + \frac{\ln[r_i/(r_i - x_d)]}{2\pi k_d L} + \frac{\ln(r_o/r_i)}{2\pi k_m L} + \frac{1}{h_c A_c} \quad (4)$$

where A_h is the area of the liquid−deposit interface, which would be A_i for a clean tube (i.e., in the absence of any deposit layer).

Temperature Difference Ratio. For wax deposition at pseudo-steady state, the temperature difference across the deposit layer is indicative of the layer's thermal resistance. A dimensionless ratio of the temperature difference across the deposit layer and the overall thermal driving force (i.e., the temperature difference between the hot and cold streams) is given by

$$\theta_d = \frac{T_d - T_{wi}}{\bar{T}_h - \bar{T}_c} \quad (5)$$

Note that θ_d is also the ratio of the thermal resistance of the deposit layer and the overall thermal resistance given by eq 4. Accordingly, θ_d can also be expressed as

$$\theta_d = \frac{R_d}{R_h + R_d + R_m + R_c} \quad (6)$$

where R_h, R_d, R_m, and R_c are the thermal resistances, as shown in eq 4, corresponding to the hot stream, the deposit layer, the tube wall, and the cold stream, respectively. That is, $R_h = [h_h A_h]^{-1}$, $R_d = \ln[r_i/(r_i - x_d)]/2\pi k_d L$, $R_m = \ln(r_o/r_i)/2\pi k_m L$, and $R_c = [h_c A_c]^{-1}$.

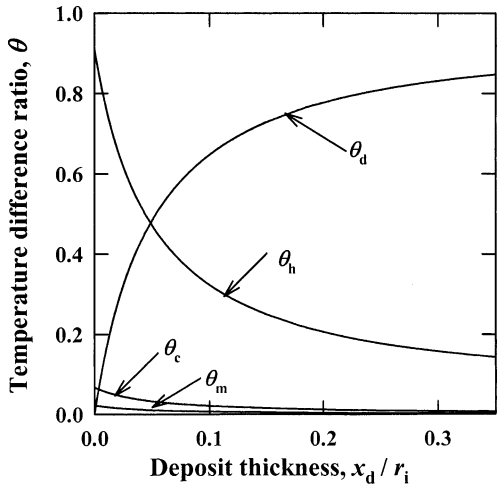

Figure 2. Comparison of the predicted relative magnitudes of thermal resistances.

To compare the magnitudes of all thermal resistances at pseudo-steady state, the heat-transfer model was used to perform calculations at the conditions of the wax deposition experiments carried out in this study. One set of model predictions is shown in Figure 2, where the dimensionless ratio, θ, for each of the individual thermal resistances is plotted against the deposit thickness, expressed as the dimensionless ratio x_d/r_i. The values of R_h, R_d, R_m, and R_c used for predictions in Figure 2 were $6.66 \times 10^{-3}(0.0132 - x_d)^{-1}$, $13.2 \ln[0.0132/(0.0132 - x_d)]$, 1.54×10^{-2}, and 4.68×10^{-2} K/W, respectively. In the absence of any solid deposition (i.e., $x_d/r_i = 0$), the thermal resistance for the hot stream is the controlling resistance, i.e., $\theta_h \gg \theta_m$, θ_c. With an increase in the thickness of the deposit layer (x_d/r_i), θ_h decreases while θ_d increases sharply. At $x_d/r_i > 0.05$, θ_d becomes the controlling resistance, resulting in the largest temperature drop across the deposit layer. That is, when the deposit thickness is greater than about 5% of the tube radius, the solid layer offers the controlling resistance in the heat-transfer process. Additional predictions from this heat-transfer model will be presented later, in the interpretation of the results obtained from the laboratory experimental program described in the following section.

Experimental Section

Materials. As mentioned previously, experiments were carried out with prepared solutions of a paraffinic wax in *n*-dodecane. The wax sample used in this study was obtained from Sigma-Aldrich (Oakville, ON, Canada). With an approximate melting point of 58−62 °C, it consisted of *n*-alkanes ranging from C_{20} to C_{40}. The wax sample was characterized further by using a simulated distillation analysis performed on an HP6890 gas chromatograph (GC) equipped with a nonpolar fused-silica column (10 m × 0.53 mm × 0.88 μm) and a hydrogen flame ionization detector (FID). The GC was calibrated using the ASTM D2887 Extended method with a C_5−C_{66} hydrocarbon standard SD-SS3E-05 (Separation Systems Inc., Gulf Breeze, FL). The results of compositional analysis on duplicate wax samples are shown in Figure 3, from which the mean carbon number was calculated to be 28. Dodecane (*n*-$C_{12}H_{26}$), with a purity of >99%, was also obtained from Sigma-Aldrich. It had a normal boiling point of 215 °C and a specific gravity

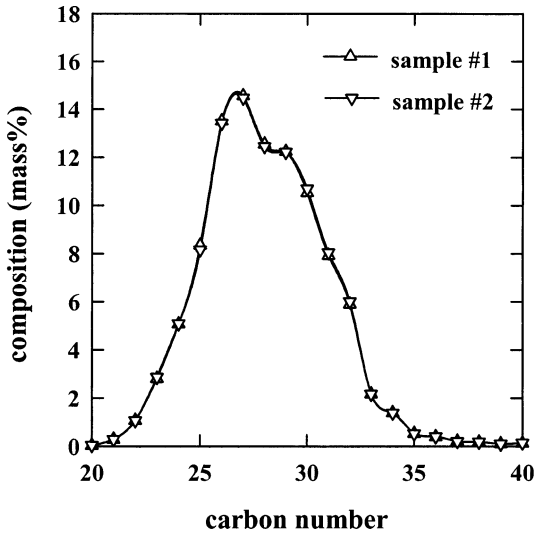

Figure 3. Carbon number distribution of the paraffin wax.

Table 1. Comparison of Measured WAT Values and Estimated Deposit−Liquid Interface Temperature

wax concentration in wax−C_{12} mixture (mass %)	WAT (°C)		estimated T_d (°C)
	visual	DSC[29]	
10	27	26.5	26
15	31	–	31
20	34	32.7	34

of 0.748. Note that *n*-dodecane (C_{12}) is essentially nonvolatile at the highest temperature of 75 °C used in this study.

WAT Measurements. The ASTM standard test method for measuring the WAT (ASTM D2500-99) involves its visual determination while a sample is cooled under a prescribed schedule. Tiwary[29] modified the method slightly by cooling the sample in steps of 1 °C and holding the sample at each constant temperature for 15 min before checking visually for the appearance of wax crystals. The WAT values for waxy crude oils have been measured using techniques such as differential scanning calorimetry (DSC) and cross-polar microscopy.[12,30−32] For prepared mixtures of wax−C_{12} and wax−C_{16}, the WAT values obtained from the modified visual method were in agreement with those from other methods; hence, the modified visual method was considered a reliable technique for WAT measurements.[29] The modified visual method was used for the WAT measurement for three wax−C_{12} mixtures with 10, 15, and 20 mass % wax. In Table 1, the WAT values from the visual method compare well with those obtained by Tiwary[29] using the DSC technique for 10 and 20 mass % wax−C_{12} mixtures.

Experimental Apparatus. The bench-scale apparatus designed for carrying out wax deposition experiments involved a novel "draft tube" assembly. The experimental setup consisted of two temperature-regulated baths, three positive displacement pumps, and three identical draft tube assemblies. A schematic of the experimental setup is shown in Figure 4. Each draft tube assembly, shown schematically in Figure 5, consisted of a cylindrical vessel, 10.2 cm in diameter, for holding a batch of the hot wax−solvent mixture. The volume of the cylindrical vessel was sufficiently large that the wax−C_{12} mixture composition did not change significantly as a result of solid deposition during the batch experiment.[33] A draft tube design to function as

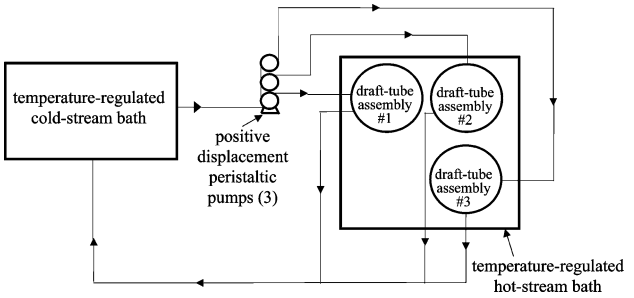

Figure 4. Experimental setup for wax deposition experiments.

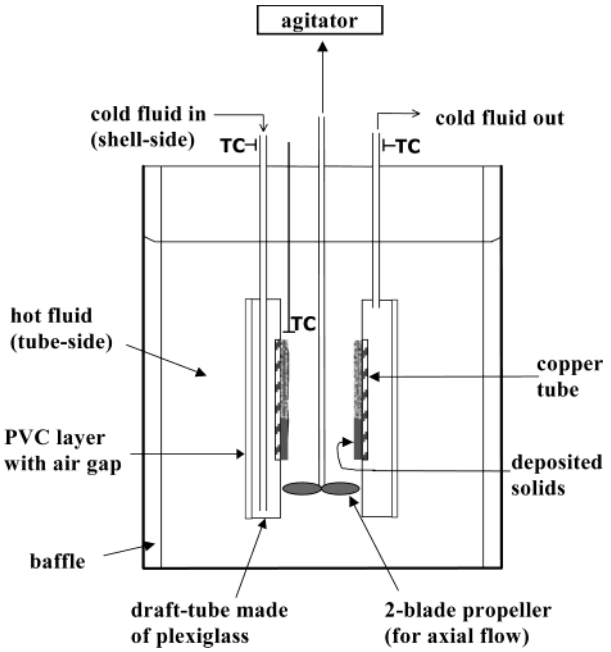

Figure 5. Schematic of the draft tube assembly.

a small heat exchanger was fitted with an axial flow propeller and inserted into the vessel. The draft tube, made of plexiglass, was designed in a concentric tube arrangement with a short copper tube embedded into its inner surface. This copper tube (26.4 mm i.d., 1.1 mm thick, and 48 mm long) provided the heat-exchange surface for the deposition of wax. No surface treatment of the commercially available copper tubing was performed. The outer wall of the draft tube was covered with a concentric PVC tube, separated by an air gap, to minimize heat transfer from the outer surface of the draft tube; calculations were made to account for the heat loss.[33] The annular region of the draft tube was used for the circulation of the cold fluid from a refrigerated circulating bath, which entered and exited the annular region at opposite ends through two narrow tubes, each fitted with a calibrated thermocouple for temperature measurements.

The axial flow propeller, driven by compressed air, was used to accomplish the circulation of the hot stream through the inner region of the draft tube. The downward flow along the propeller shaft caused the hot stream to circulate through the inner tube of the draft tube assembly. Another flow apparatus was used for calibrating the hot fluid flow rate with the propeller speed at ambient temperature.[33] A thermocouple was placed below the copper tube for measuring the outlet hot-stream temperature; however, this thermocouple was removed because of its interference with the rotating propeller. With the deposit layer thickness being

Table 2. Regression Constants for Determining Heat-Transfer Coefficient, U_i, from Eq 8

wax concentration (mass %)	α $(m^2 \cdot K/W)(m^3/s)^{\beta}$	β	δ $(m^2 \cdot K/W)(m^3/s)^{\eta}$	η
10	$(2.11 \pm 0.13) \times 10^{-4}$	0.231 ± 0.060	9×10^{-13}	1.49 ± 0.50
15	$(4.44 \pm 0.93) \times 10^{-5}$	0.375 ± 0.090	9×10^{-13}	1.59 ± 1.08
20	$(6.31 \pm 0.21) \times 10^{-4}$	0.113 ± 0.040	9×10^{-13}	1.53 ± 1.20

3 mm or less in all experiments, the effect of this layer on the hot fluid flow rate and the heat-transfer coefficient calculation was assumed to be negligible. Two circulation rates for the hot stream were used, and the corresponding shear rates at the tube wall were estimated to be 6.4 and 26 s^{-1}.[33] A calibrated thermocouple was placed at the top of the inner tube, just above the copper tube insert.

Each vessel, fitted with one draft tube assembly, was placed into a second temperature-regulated water bath. The vessels were filled with the prepared wax−C_{12} mixture as the hot stream. The agitator was turned on to circulate the solution through the draft tube, allowing the wax−C_{12} mixture to reach the preset hot-stream temperature. To commence an experiment, the positive displacement pump was turned on to start the circulation of the cold (water) stream from the refrigerated bath at a constant flow rate through the annular region of the draft tube. Thus, the inner surface of the copper tube was exposed to the wax−C_{12} mixture and the outer surface to cold water. The deposition of solids occurred on the inner surface of the copper tube imbedded in the draft tube.

Heat-Transfer Coefficients for the Draft Tube. Because of the short tube length used in the draft tube assembly, existing correlations for heat-transfer coefficients were not applicable. Instead, the following empirical approach was adapted for estimating the heat-transfer coefficients: The convective heat-transfer coefficient for the hot and cold streams, h, was assumed to be a function of the Reynolds number, Re; the Prandtl number, Pr; and the ratio z/D, and it was expressed as

$$\frac{hD}{k} = C\, Re^m\, Pr^n (z/D)^p \tag{7}$$

where D is the tube diameter; z is the axial distance; k is the fluid thermal conductivity; and C, m, n, and p are constants that usually depend on the flow regime, the fluid properties, and the geometry. Over the narrow temperature changes involved in our experiments, average properties of both the hot and cold fluids were used. The values of z ($\equiv L$) and D were the same for all experiments. The term $(z/D)^p$ and all fluid properties, including Pr, were combined into the proportionality constant C in eq 7 for each wax−C_{12} mixture and the cold stream. That is, h was expressed as a function of only the flow rate (or fluid velocity) for both the hot and cold streams, i.e., $h \propto F^m$. With $A_i \equiv A_h$ and $A_o \equiv A_c$, eq 4 was expressed as follows

$$\frac{1}{U_i} = \frac{\alpha}{F_i^{\beta}} + \frac{A_i}{A_o}\frac{\delta}{F_o^{\eta}} + A_i R_m \tag{8}$$

where F_i (hot) and F_o (cold) are the inside and outside fluid flow rates, respectively. Constants α, β, δ, and η in eq 8 were determined from experiments performed at temperatures that did not result in the precipitation or deposition of wax solids. Further details of these calibration experiments, all of which were performed with both the cold- and hot-stream temperatures above the WAT of the three wax−C_{12} mixtures, are given by Bidmus.[33]

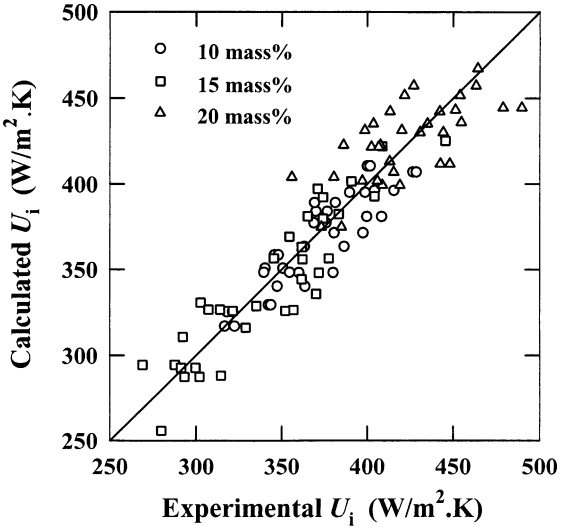

Figure 6. Comparison of experimental and calculated values of the overall heat-transfer coefficient.

A regression analysis was performed on the data from a large number of calibration experiments using the three wax−C_{12} solutions to obtain the four constants in eq 8, which are listed in Table 2. A comparison of experimental and calculated values of U_i is shown in Figure 6. The data were found to fit eq 8 with a correlation coefficient (r^2) of 0.84, which was considered to be acceptable, especially given the fact that the relatively small thermal resistances for the two convective terms did not control the rate of heat transfer in most wax deposition experiments.

Wax Deposition Experiments. As mentioned previously, three compositions of 10, 15, and 20 mass % wax in wax−C_{12} mixtures were used in the wax deposition experiments. About 660 mL of a wax−C_{12} mixture was preheated to 70 °C and poured into each vessel placed in the higher-temperature bath. The wax−C_{12} mixture was then cooled at a constant cooling rate of 25 °C/h to the hot-stream temperature for the experiment. The circulation of the cold stream was commenced through the draft tube to begin the deposition experiment. To terminate the experiment, the agitator was turned off, and the draft tube was lifted out of the cylindrical vessel, after which the cold-stream flow was turned off. The draft tube was dismantled carefully to isolate the copper tube with the deposited solid. The mass of the deposit was determined by difference, and a sample of the deposit was saved for GC analysis.

Design of Wax Deposition Experiments. To investigate the effects of various variables on the wax deposition process, a factorial design of experiments was implemented with three levels of wax−C_{12} mixture composition, three levels of the hot-stream temperature, three levels of the cold-stream temperature, and two levels of the hot-stream shear rate. With each wax−C_{12} mixture, experiments were performed with a hot-

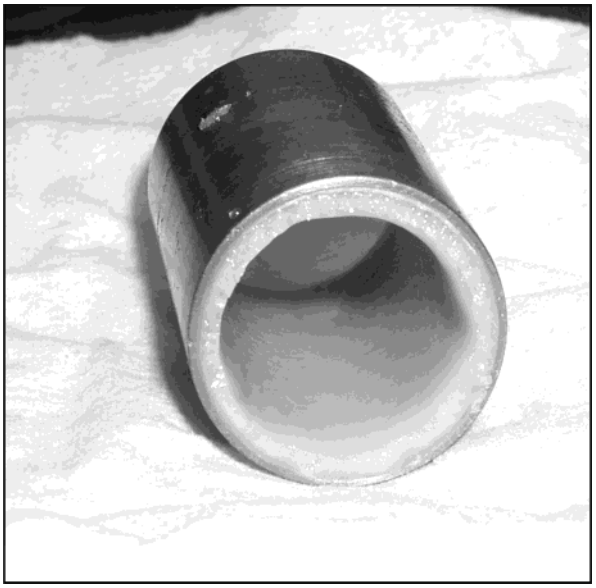

Figure 7. Copper tube with typical wax deposit on inner surface.

stream temperature that was 5, 10, or 15 °C above the WAT while the cold-stream temperature was maintained at 5, 10, or 15 °C below the WAT. Each wax deposition experiment involved running all three draft tube assemblies for three residence times of 30, 60, and 120 min. Additional experiments with wax−C_{12} mixtures were performed to verify the reproducibility of the experimental measurements, and experiments were also conducted for longer residence times of 240−720 min to investigate the effect of extended deposition times.[33]

Hydrodynamic Entry Region Considerations. In the heat-transfer model, the deposit layer thickness was assumed to be uniform over the tube length. Figure 7 is a photograph of the copper tube with deposited wax, which shows the deposit layer to be nearly uniform over the tube length. In all experiments, there was no evidence of any impact of hydrodynamic entry length effects on wax deposition.[33]

Results and Discussion

Detailed results of the large number of wax deposition experiments, performed according to the design of experiments, have been reported by Bidmus.[33] In the following sections, these experimental results are discussed and compared with predictions from the heat-transfer model.

Thermal Pseudo-Steady State. As mentioned previously, the heat-transfer model was developed on the assumption of a thermal pseudo-steady state; therefore, it was necessary to ensure that all of the temperatures reached constant values in each wax deposition experiment. For this purpose, all thermocouple readings were recorded using a data logger. Figure 8 shows typical results for the difference between the outlet and inlet cold-stream temperatures, $T_{c-out} - T_{c-in}$, with time at both shear rates for the three wax−C_{12} mixtures. The overall thermal driving force, $\bar{T}_h - \bar{T}_c$, for all of the results in Figure 8 was approximately 30 °C. It is evident that a thermal steady state at both shear rates of 6.4 and 26 s^{-1} was reached within about 20 min. Similar trends were observed from temperature records of all wax deposition experiments. It was observed that the mass of the deposit layer did not vary with the residence time over the range of 30−120 min.[33] At

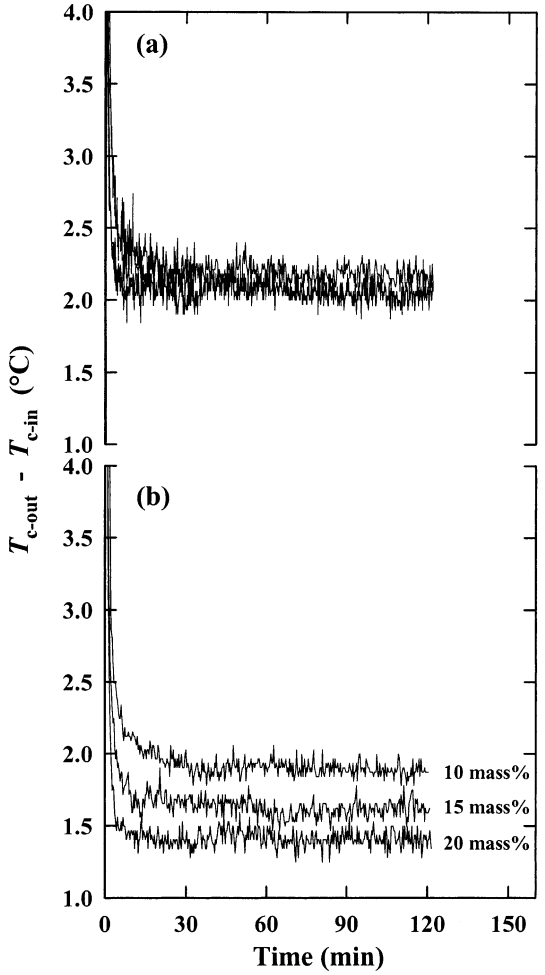

Figure 8. Approach to thermal steady state in wax deposition experiments: (a) shear rate = 26 s^{-1}, (b) shear rate = 6.4 s^{-1}.

similar values of the hot- and cold-stream temperatures, a higher wax concentration in wax−C_{12} mixtures yielded a higher mass of deposited solid.[33]

The amount of deposited solid was expressed as the mass of deposit per unit inside tube surface area, Ω, which is related to the deposit layer thickness, x_d, as follows

$$\Omega = \frac{\text{mass of deposit}}{\text{tube inside surface area}} = \frac{r_i^2 - (r_i - x_d)^2}{2\,r_i}\rho_d = \left(x_d - \frac{x_d}{r_i}\frac{x_d}{2}\right)\rho_d \quad (9)$$

where ρ_d is the density of the deposit. Note that the thermal resistance of the deposit layer depends on Ω (related to x_d by eq 9) and k_d, i.e., $R_d = \ln[r_i/(r_i - x_d)]/2\pi k_d L$.

Effect of the Hot- and Cold-Stream Temperatures. Typical results for the effect of the average hot-stream temperature on the deposit mass, for a constant cold-stream temperature, are plotted in Figure 9. All of the curves in Figure 9 represent values predicted using the heat-transfer model, which are seen to compare well with the experimental results. Note that the abscissa in Figure 9 represents the difference between the average hot-stream temperature and the corresponding value of the WAT for the wax−C_{12} mixture. In Figure 9, Ω increases in all cases with a decrease in ($\bar{T}_h$ − WAT), which implies that wax deposition increases as

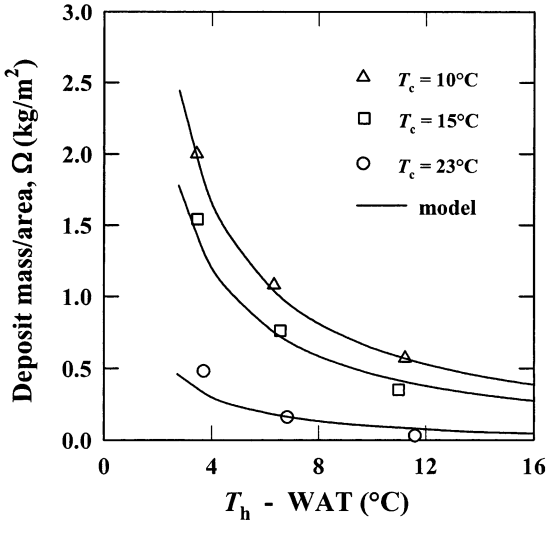

Figure 9. Effect of the hot-stream (wax−C_{12} mixture) temperature on wax deposition for the 10 mass % mixture at three cold-stream temperatures and a shear rate of 26 s^{-1}.

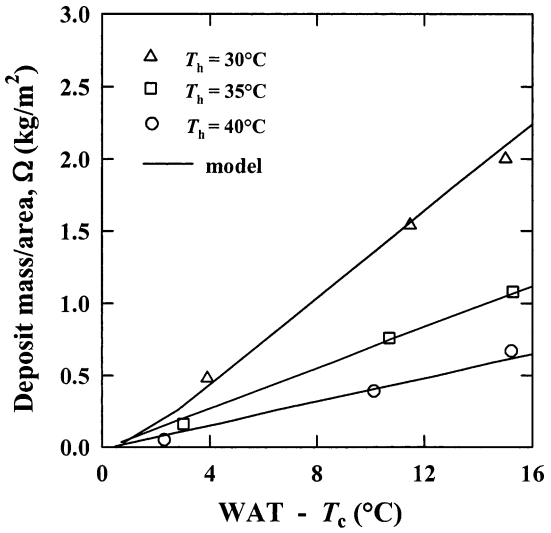

Figure 10. Effect of the cold-stream temperature on wax deposition for the 10 mass % mixture at three hot-stream temperatures and a shear rate of 26 s^{-1}.

the hot-stream temperature approaches the WAT. Also, higher values of Ω are achieved at lower cold-stream temperatures because of the larger thermal driving force.

The results shown in Figure 9 are replotted in Figure 10 to highlight the effect of the cold-stream temperature. In Figure 10, Ω is plotted against the difference between the WAT and the average cold-stream temperature, and the relationship between Ω and (WAT − $\bar{T}_c$) is observed to be essentially linear. The value of Ω approaches zero as the cold-stream temperature approaches the WAT of the wax−C_{12} mixtures, i.e., the cold-stream temperature must be less than the WAT in order for wax deposition to take place. Again, predictions from the heat-transfer model are in good agreement with the experimental results.

Effect of the Overall Thermal Driving Force. Figure 11 presents the effect of overall thermal driving force, $\bar{T}_h - \bar{T}_c$, on Ω for 10 and 15 mass % wax−C_{12} mixtures at the same shear rate of 26 s^{-1}. Note that the results for the 10 mass % mixture are shown in Figure 11 as open symbols, and for 15 mass % mixture as solid symbols. With the hot-stream temperature held

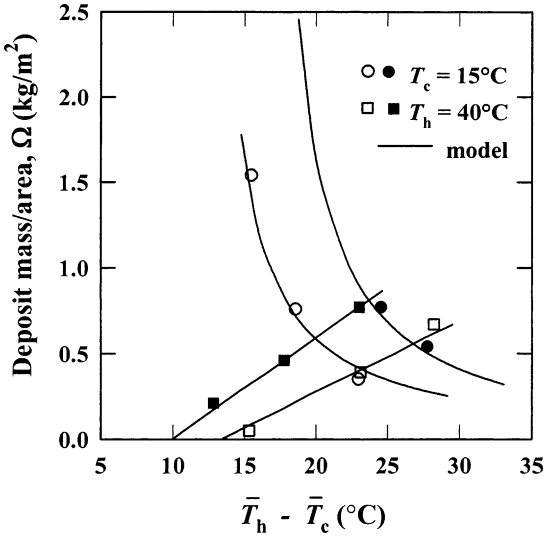

Figure 11. Effects of the overall thermal driving force and hot-/cold-stream temperatures in wax deposition from 10 and 15 mass % mixtures at a shear rate of 26 s^{-1} (open symbols, 10 mass % mixture; solid symbols, 15 mass % mixture).

at 40 °C, an increase in the overall thermal driving force (obtained by lowering the cold-stream temperature) resulted in a linear increase in Ω. However, the result was opposite when the overall thermal driving force was increased by increasing the hot-stream temperature. In experiments with the cold-stream temperature held at 15 °C, an increase in the overall thermal driving force resulted in a sharp decrease in Ω.

Several studies on wax deposition from waxy crude oils have reported an increased amount of wax deposition with an increase in the temperature difference between the crude oil and the cold surface temperature.[7,8,10,16,22] However, this result was based on experiments performed either by varying the coolant/wall temperature while keeping the oil temperature constant or by changing both the oil and coolant/wall temperatures simultaneously. As shown in Figure 11, the amount of wax deposition depends not only on the overall thermal driving force but also on the individual values of the hot- and cold-stream temperatures. These results confirm the findings of Ghedamu et al.[27]

Effect of θ_d. In eqs 5 and 6, the temperature difference ratio, θ_d, is shown to be equal to the ratio of the thermal resistance offered by the deposit layer to the sum of four thermal resistances in series. For the results of all wax deposition experiments, calculations were performed for the deposit quantity, Ω, as well as the corresponding θ_d values from eq 6. The results are plotted in Figure 12 for all three wax−C_{12} mixture compositions at both shear rates, for all combinations of hot-/cold-stream temperatures, and for all residence times of 30−120 min. Also shown in Figure 12 is the curve representing the model predictions at the higher shear rate, which matches the data very well. It is noted that model predictions for the dependence of the wax deposit amount on θ_d were similar for the three wax−C_{12} mixture compositions investigated.[33]

A number of other observations can be made from Figure 12. The amount of wax deposit increases with an increase in θ_d. Figure 12 also confirms that no wax deposition occurs when $\theta_d = 0$, which is expected because $\theta_d = 0$ implies $R_d = 0$ and, hence, no temperature drop across the deposit layer. Also, the amount

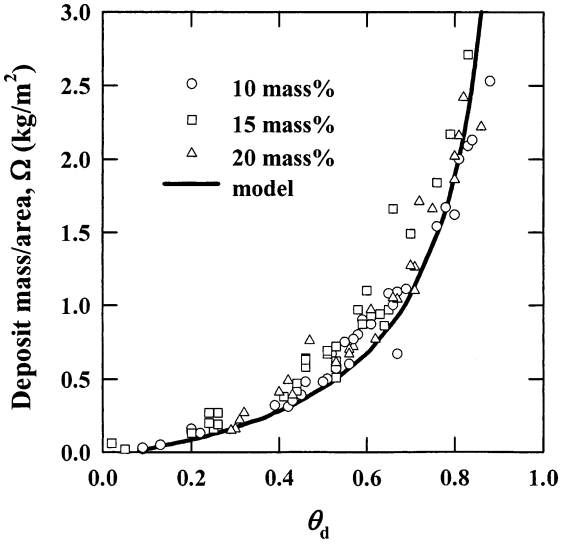

Figure 12. Dependence of wax deposition on θ_d; model predictions at a shear rate of 26 s^{-1} shown by smooth curve.

of wax deposited at constant θ_d was the same for all three compositions.

The results in Figure 12 establish θ_d as an important parameter for describing the amount of wax deposition. Because θ_d is indicative of the fractional thermal resistance as well as the fractional temperature drop across the deposit layer, the deposition of wax from wax−solvent mixtures is dependent primarily on the rate of heat transfer.

Deposition Experiments without a Thermal Driving Force. Additional wax deposition experiments were performed with no temperature difference between the hot and cold streams. All of these experiments were carried out at hot-stream temperatures that were below the respective WAT of each wax−C_{12} mixture but without any circulation of the cold stream, which made the hot- and cold-stream temperatures have the same value at steady state. A total of nine such experiments, three for each wax−C_{12} mixture composition, were performed at the shear rates of 6.4 and 26 s^{-1}, as well as under conditions of no shear rate (i.e., no circulation of the wax−C_{12} mixture).

In all of these experiments, despite the presence of solid particles suspended in the wax−C_{12} mixture held at a temperature below the WAT, no solid deposition was observed even after a residence time of 120 min. Thus, the presence of suspended wax particles in wax−C_{12} mixtures will not lead to solid deposition unless a thermal driving force is introduced between the hot wax−C_{12} mixture and the cold surface (held at a temperature below the WAT).

Estimation of the Liquid−Deposit Interface Temperature. One of the assumptions made in developing the heat-transfer model was that the liquid−solid interface temperature between the hot wax−C_{12} mixture and the deposit layer was equal to the WAT. This assumption was used in solving the set of heat-transfer equations, predictions from which were shown to compare well with the results from wax deposition experiments. To verify this assumption further, additional optimization calculations with the heat-transfer model were made as follows: For a given wax−C_{12} mixture composition, experimental values of the hot- and cold-stream temperatures and Ω, along with an assumed value of the interface temperature, T_d, were used to

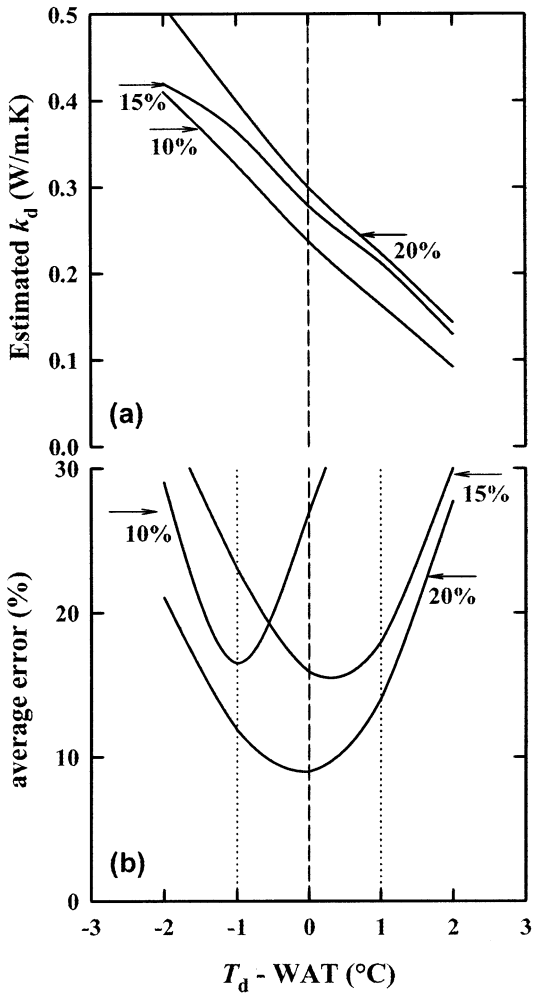

Figure 13. Optimum results for the hot-stream−deposit interface temperature (T_d) and the wax deposit layer thermal conductivity (k_d).

solve eqs 2, 3, and 9 for x_d and k_d for one experiment This calculation was repeated for all experiments with the same wax−C_{12} mixture composition to obtain the optimum value of k_d that gave the best overall match of the results from all experiments The corresponding value of Ω was calculated and compared with the experimental value. A relative error was calculated as follows

$$\% \text{ error} = 100 \times \frac{|\Omega_{calc} - \Omega_{expt}|}{\Omega_{expt}} \qquad (10)$$

An average value of % error was obtained for all experiments with the same wax−C_{12} mixture. The calculations for x_d, Ω, k_d, and % error were repeated with other assumed values of the interface temperature, T_d. Finally, these calculations were repeated for experimental data from the other two wax−C_{12} mixture compositions.

Figure 13 presents the results of these optimization calculations for all three mixtures at the shear rate of 26 s^{-1}. Note that each curve in Figure 13b shows a region of minimum percentage error that is within ±1 °C of the WAT value. The best values of T_d, corresponding to the minima in Figure 13b, are listed in Table 1, and these agree with the measured WAT values.

Figure 13a shows the corresponding "optimum" values of k_d to be within a range of 0.2−0.3 W/m·K. With the

thermal conductivities of C_{12} and paraffin waxes taken as 0.17 and 0.24 W/m·K, respectively, the thermal conductivity of the deposit would be expected to be between these values. However, the deposit layer is a heterogeneous mixture of solid wax and liquid wax−C_{12} mixture that is under a temperature gradient, which affects the solid-to-liquid ratio and the composition over the layer thickness. In addition, the liquid phase trapped in the deposit layer might possibly give rise to convective effects within the deposit layer, which would yield an increase in the value of k_d. In view of these effects, the optimum range of 0.2−0.3 W/m·K is a reasonable estimate of k_d.

The fact that the results of the wax deposition experiments along with a model based on heat transfer provide reasonable estimates of both the WAT and k_d offers further confirmation that the wax deposition process at pseudo-steady state is governed primarily by the rate of heat transfer.

Compositional Analysis of the Wax Deposits

Although the main objective of this study was to investigate the role of heat transfer in solids deposition from wax−solvent mixtures, this section presents GC analysis results on the samples collected from solid deposition experiments. Note that the gel-like deposited solids consisted of two phases: a solid phase with wax/paraffin constituents (C_{20}−C_{40}) and a liquid phase with paraffins dissolved in C_{12}.

All GC analyses were performed using the previously described simulated distillation technique. The carbon number distribution was determined for the initial and final liquid wax−C_{12} mixtures, as well as for the three deposit samples collected at different residence times during each wax deposition experiment. The GC analyses of the initial and final wax−C_{12} mixtures were very similar in all cases, which confirmed the assumption that the mixtures did not undergo any significant change in the wax concentration during the solid deposition experiments.[33] The volume of deposited solids ranged from 0.4 to 12 mL in most experiments, compared to 660 mL of the wax−C_{12} mixture used in each draft tube assembly.

Results for 10 Mass % Wax−C_{12} Mixtures. The GC analysis results in this section are for samples collected from solids deposition experiments conducted with 10 mass % wax−C_{12} mixtures.

Paraffin Content of the Deposit. Figure 14 presents the carbon number distribution, normalized on a C_{12}-free basis, for the three deposit samples at different residence times, as well as for the initial wax−C_{12} mixture. These results are for the samples collected from the experiment with the 10 mass % wax−C_{12} mixture at a shear rate of 26 s^{-1}.

For relatively low wax concentrations in wax−C_{12} mixtures (i.e., 10−20 mass % wax), it is expected that a small error in GC analysis for C_{20+} paraffin constituents will be amplified when the results are expressed on a C_{12}-free basis. This would explain the small discrepancy between the carbon number distribution for "pure" wax in Figure 3 and that for the wax−C_{12} mixture in Figure 14. It can be observed from Figure 14 that, with an increase in residence time, the carbon number distributions shift to the right. Similar trends were observed for other experiments with the 10 mass % wax−C_{12} mixture.[33]

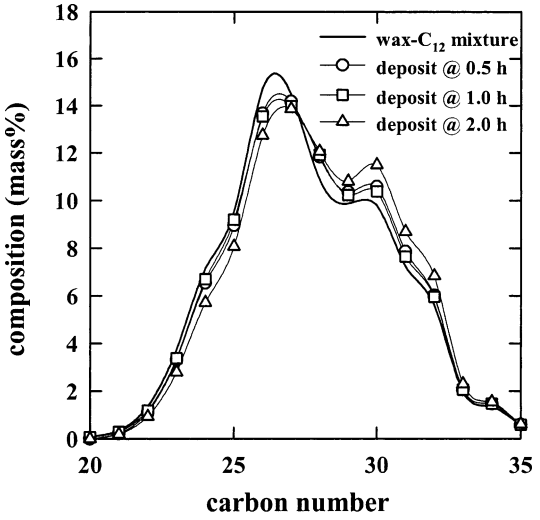

Figure 14. Changes in carbon number distribution with residence time for the 10 mass % mixture at a shear rate of 26 s^{-1}.

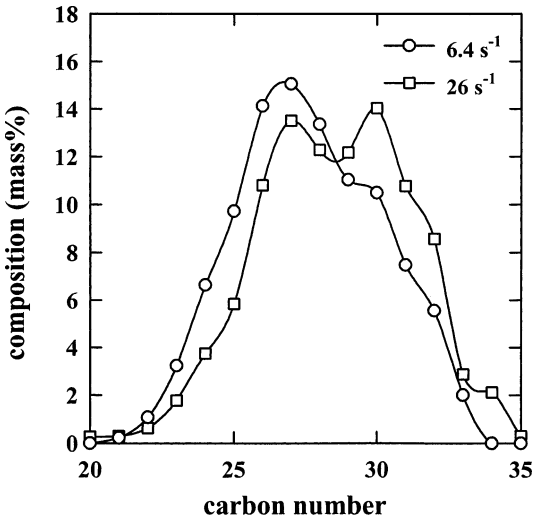

Figure 15. Comparison of carbon number distribution for solid deposits from the 10 mass % mixture at shear rates of 6.4 and 26 s^{-1}.

Compared to the carbon number distribution for the wax−C_{12} mixture in Figure 14, all of the deposit samples had lower concentrations of *n*-alkanes below C_{28} and higher concentrations of *n*-alkanes above C_{28}. In other words, with increasing residence time, molecules of *n*-alkanes heavier than C_{28} diffused into the deposited solid and molecules lighter than C_{28} diffused out of the deposit. Using the definition proposed by Singh et al.,[6] the critical carbon number for the wax−C_{12} system used in this study was found to be 28. As mentioned previously, the mean carbon number of the wax sample used in this study was also 28.

Effect of Shear Rate on Paraffin Content. The carbon number distributions for the solid deposits obtained from two experiments that differed only in the shear rate are compared in Figure 15. Between the results for the two shear rates, the deposits obtained at the higher rate of shear of 26 s^{-1} also had a higher concentration of *n*-alkanes heavier than C_{28}. The wax deposits obtained at the lower shear rate were noted to be softer and more loosely bonded than those at the higher shear rate.[33]

Wax and C_{12} Contents of the Deposit. As mentioned previously, the wax deposit is a gel-like structure

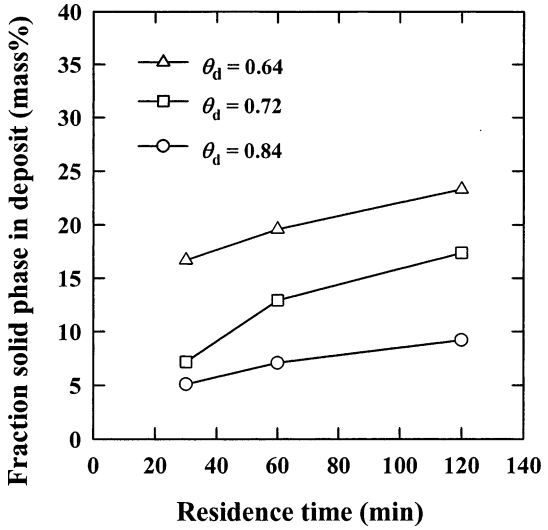

Figure 16. Increase of solid-phase fraction in the wax deposit with residence time for the 10 mass % mixture at a shear rate of 26 s^{-1}.

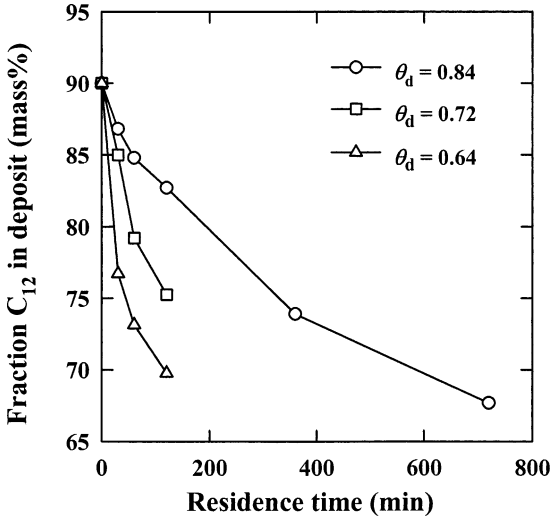

Figure 17. Variation of C_{12} content in the wax deposit with residence time and θ_d for the 10 mass % mixture at a shear rate of 26 s^{-1}.

comprising a solid phase with wax constituents (C_{20}−C_{40}) and a liquid phase with wax dissolved in C_{12}. The analyses presented so far were based on the *n*-alkane content of the entire deposit, including the portion dissolved in the wax−C_{12} liquid phase entrapped in the gel-like structure. A mass balance calculation was used to estimate the *n*-alkane content in the solid phase of deposited solids. This calculation was based on the assumption that the composition of liquid entrapped in the deposit layer was identical to the composition of the bulk wax−C_{12} mixture.

The estimated values of the solid-phase content in the deposits from experiments with 10 mass % wax−C_{12} mixtures are shown in Figure 16. These results show interesting trends with residence time as well as θ_d. The fraction of solid phase increases with increasing residence time, which implies that the liquid phase entrapped in the gel-like deposit is replaced with the solid phase. Interestingly, the solid-phase fraction is higher at lower values of θ_d, which corresponds to a relatively lower fractional thermal resistance offered by the deposited layer.

For the same set of wax deposition experiments, Figure 17 shows a decrease in the C_{12} content of the deposit layer with residence time and θ_d. As expected, the concentration of C_{12} in the deposit layer decreases with time. An interesting observation in Figure 17 is that, for the same residence time, the C_{12} concentration decreases with decreasing θ_d. Note that the experiment at $\theta_d = 0.84$ was performed twice; once for residence times of 0.5−2 h and then again for longer residence times up to 12 h. At $\theta_d = 0.84$, the C_{12} concentration after 720 min was about the same as that at $\theta_d = 0.64$ after 120 min. This implies that the rate of decline of the C_{12} concentration in the deposit layer is faster at lower values of θ_d. It was shown previously that the deposit mass increases with θ_d and that higher shear rates increase the solid content of the deposit, leading to the aging of the wax deposit. Therefore, these experimental results suggest that the operating conditions that give a thinner deposit layer also favor an increase in the solid content of the deposit. Clearly, the interactions between the solid and liquid phases in the waxy deposit are complex and require further investigation.

Results for 15 and 20 Mass % Wax−C_{12} Mixtures. The results in the previous section were for samples from experiments with 10 mass % wax−C_{12} mixtures. Similar GC analyses and calculations were performed on samples from experiments with 15 and 20 mass % wax−C_{12} mixtures, which gave trends that were different from those for 10 mass % wax−C_{12} mixtures.

Plots a and b of Figure 18 show the carbon number distributions in solid deposits, on a C_{12}-free basis, obtained from 15 and 20 mass % wax−C_{12} mixtures, respectively. Unlike Figure 14, there is no noticeable difference between the carbon number distributions for the wax−C_{12} mixture and the three deposits at either wax concentration. For all carbon numbers, the composition differences between the liquid wax−C_{12} mixtures and solid deposits were within ±0.5 mass %. Furthermore, the carbon number distribution in the deposit did not show an appreciable change even after a residence time of 12 h, as shown in Figure 18b for the 20 mass % wax−C_{12} mixture. Similar results were obtained for all solid deposit samples with 15 and 20 mass % wax−C_{12} mixtures.[33]

In Figure 19, the estimated values of the fraction of C_{12} in the deposit from 20 mass % wax−C_{12} mixtures are seen to decrease only slightly with residence time. Similar results were observed in experiments with 15 mass % wax−C_{12} mixtures. The results in Figure 19 suggest that the rate at which the solid content of the deposit changes with time is slower for the 20 mass % mixture than that for the 10 mass % mixture shown in Figure 17. One possible explanation for the lack of any noticeable change in the solid content could be a slower aging of the deposits from mixtures with higher wax concentrations. In that case, deposition experiments performed over longer residence times might show a change in the composition of deposited solids and/or the fraction of the solid phase. That is, experiments with higher wax concentrations in solvent(s), carried out over longer residence times, might explain the observed compositional differences in solid deposits from 10 and 15−20 mass % wax−C_{12} mixtures.

Conclusions

A steady-state heat-transfer model was developed and validated experimentally for the wax deposition process.

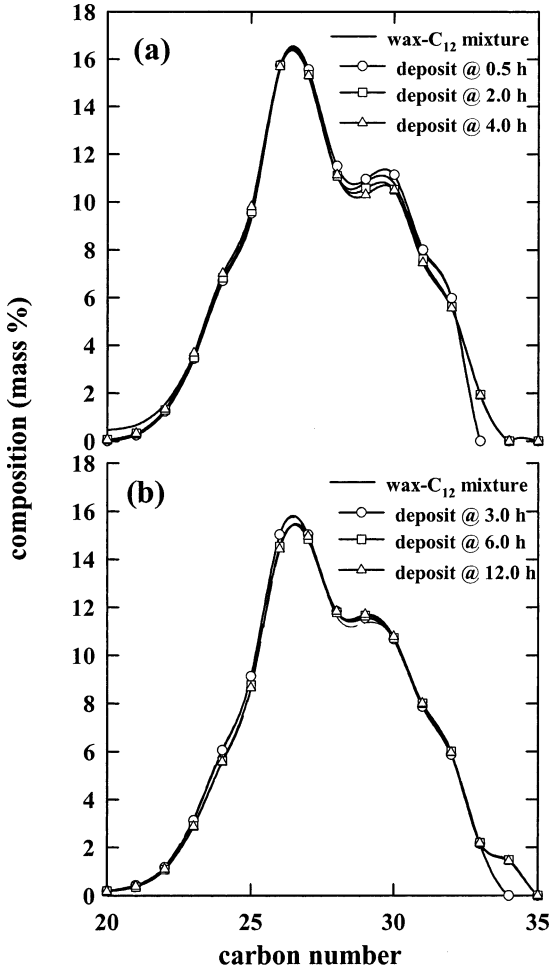

Figure 18. Comparison of carbon number distributions for solid deposits at a shear rate of 26 s^{-1}: (a) 15 mass % mixture, θ_d = 0.65; (b) 20 mass % mixture, θ_d = 0.71.

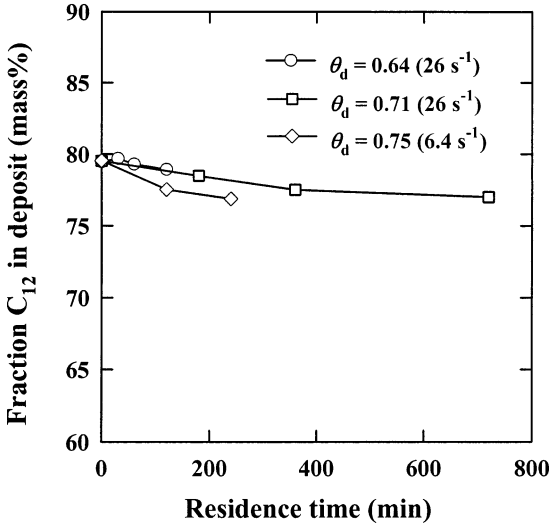

Figure 19. Variation of C_{12} content in wax deposit with residence time and θ_d for 20 mass % mixture at shear rates of 6.4 and 26 s^{-1}.

The amount of deposited waxy solid was related to a single parameter, θ_d, which is the ratio of the temperature drop across the deposit layer to the overall thermal driving force. Parameter θ_d is also the ratio of the thermal resistance of the deposit layer to the overall thermal resistance for heat exchange between the hot and cold streams. The deposit layer was shown to offer the controlling thermal resistance even at relatively small deposit thicknesses. It was shown that, under thermal pseudo-steady state, the deposit−liquid interface is at the wax appearance temperature (WAT) of the wax−solvent mixture. On the basis of an extensive comparison of experimental results with the heat-transfer model predictions, the wax deposition process was established to be dominated primarily by the rate of heat transfer.

An apparatus incorporating a novel draft tube assembly was designed for investigating the deposition of waxy solids from prepared solutions of a paraffinic wax in *n*-dodecane (C_{12}). The bench-scale draft tube assembly was used to perform wax deposition experiments in batch mode. Experiments were carried out for the effects of the wax−C_{12} mixture composition, shear rate, hot- and cold-stream temperatures, and residence time. The wax deposition results showed that a thermal pseudo-steady state was attained within about 20 min. The amount of wax deposited was found to increase with increasing wax content of the wax−C_{12} mixture, as well as with decreasing hot- and cold-stream temperatures. That is, the mass of deposited solid was not necessarily proportional to the difference between the hot- and cold-stream temperatures.

The solid deposits and wax−C_{12} mixtures were analyzed using a simulated distillation GC technique. For the deposits from 10 mass % wax−C_{12} mixtures, the concentration of *n*-alkanes with carbon numbers below 28 decreased with time, whereas the concentration of *n*-alkanes with carbon numbers above 28 increased with time. The solid-phase content of the deposit increased with residence time. For wax−C_{12} mixtures containing the higher wax concentrations of 15 and 20 mass %, however, the composition of the deposit layer did not vary significantly over residence times up to 12 h.

Acknowledgment

Financial support from the Natural Sciences and Engineering Research Council of Canada (NSERC); DB Robinson Research Ltd., Edmonton, Canada; and the Department of Chemical and Petroleum Engineering, University of Calgary, Calgary, Alberta, Canada, is gratefully acknowledged. We thank Ms. E. Zalewski of the In Situ Combustion Group at the University of Calgary for GC analyses.

Note Added after ASAP Posting

This article was originally posted on 12/30/03 with minor inaccuracies in refs 11, 13, 18, 30, and 31. It was reposted on 1/8/04 with corrections to these references and with minor changes to the text labels in Figures 4 and 5.

Nomenclature

A_c = tube surface area in contact with the cold stream, m^2
A_i = inside surface area of the tube, m^2
A_h = area of the hot stream−deposit interface, m^2
C_c = specific heat capacity of the cold stream, J/kg·K
C_h = specific heat capacity of the hot stream, J/kg·K
D = tube diameter, m
F_i = flow rate of the hot stream, m^3/s
F_o = flow rate of the cold stream, m^3/s
h_c = heat-transfer coefficient of the cold stream, $W/m^2·K$
h_h = heat-transfer coefficient of the hot stream, $W/m^2·K$
k_d = thermal conductivity of the deposit, W/m·K

k_m = thermal conductivity of the tube wall, W/m·K
L = length of the tube, m
m = exponent in eq 7
m_c = mass flow rate of the cold stream, kg/s
m_h = mass flow rate of the hot stream, kg/s
n = exponent in eq 7
p = exponent in eq 7
Pr = Prandtl number
q = rate of heat transfer, W
R_c = thermal resistance of the cold stream, K/W
R_d = thermal resistance of the deposit layer, K/W
R_h = thermal resistance of the hot stream, K/W
R_m = thermal resistance of tube wall, K/W
Re = Reynolds number
r_i = inside tube radius, m
r_o = outside tube radius, m
T_c = temperature of the cold stream, °C
T_d = temperature at the hot stream−deposit interface, °C
T_h = temperature of the hot stream, °C
T_{c-in} = inlet temperature of the cold stream, °C
T_{c-out} = outlet temperature of the cold stream, °C
T_{h-in} = inlet temperature of the hot stream, °C
T_{h-out} = outlet temperature of the hot stream, °C
T_{wi} = temperature at the inside tube surface, °C
T_{wo} = temperature at the outside tube surface, °C
$\bar{T}_c$ = average temperature of the cold stream, °C
$\bar{T}_h$ = average temperature of the hot stream, °C
U_i = overall heat-transfer coefficient based on inside area, W/m²·K
x_d = deposit layer thickness, m
z = axial distance (≡ L), m

Greek Letters

α = coefficient in eq 8, (m²·K/W)(m³/s)$^{\beta}$
β = exponent in eq 8
δ = coefficient in eq 8, (m²·K/W)(m³/s)$^{\eta}$
η = exponent in eq 8
ρ_d = density of the deposit, kg/m³
θ_c = ratio of coolant (convective) thermal resistance to total thermal resistance
θ_d = ratio of the deposit (conductive) thermal resistance to total thermal resistance
θ_h = ratio of wax−C_{12} mixture (convective) thermal resistance to total thermal resistance
θ_m = ratio of tube-wall (conductive) thermal resistance and total thermal resistance
Ω = mass of deposit per unit inside tube surface area, kg/m²

Literature Cited

(1) Azevedo, L. F. A.; Teixeira, A. M. A Critical Review of the Modeling of Wax Deposition Mechanisms. Presented at the AIChE 2002 Spring National Meeting, New Orleans, LA, 10−14 Mar, 2002.

(2) Holder, G. A.; Winkler, J. Wax Crystallization from Distillate Fuels. I. Cloud and Pour Phenomena Exhibited by Solutions of Binary *n*-Paraffin Mixtures. *J. Inst. Pet.* **1965**, *51*, 228.

(3) Dirand, M.; Chevallier, V.; Provost, E.; Bouroukba, M.; Petitjean, D. Multicomponent Paraffin Waxes and Petroleum Solid Deposits: Structural and Thermodynamic State. *Fuel* **1998**, *77*, 1253.

(4) Holder, G. A.; Winkler, J. Wax Crystallization from Distillate Fuels. II. Mechanism of Pour Depression. *J. Inst. Pet.* **1965**, *51*, 235.

(5) Singh, P.; Venkatesan, R.; Fogler, H. S.; Nagarajan, N. Formation and Aging of Incipient Thin Film Wax−Oil Gels. *AIChE J.* **2000**, *46*, 1059.

(6) Singh, P.; Youyen, A.; Fogler, H. S. Existence of a Critical Carbon Number in the Aging of a Wax−Oil Gel. *AIChE J.* **2001**, *47*, 2111.

(7) Bott, T. R.; Gudmunsson, J. S. *Deposition of Paraffin Wax from Flowing Systems*; Report IP 77-007; Institute of Petroleum: London, U.K., 1977.

(8) Creek, J. L.; Lund, H. J.; Brill, J. P.; Volk, M. Wax Deposition in Single Phase Flow. *Fluid Phase Equilib.* **1999**, *158−160*, 801.

(9) Jessen, F. W.; Howell, J. N. Effect of Flow Rate on Paraffin Accumulation in Plastic, Steel, and Coated Pipe. *Pet. Trans. AIME* **1958**, *213*, 80.

(10) Wu, C.; Creek, J. L.; Wang, K.; Carlson, R. M.; Cheung, S.; Shuler, P. J.; Tang, Y. Measurement of Wax Deposition in Paraffin Solutions. Presented at the AIChE 2002 Spring National Meeting, New Orleans, LA, Mar 10−14, 2002.

(11) Brown, T. S.; Niesen, V. G.; Erickson, D. D. The Effects of Light Ends and High Pressure on Paraffin Formation. Presented at the SPE Annual Technical Conference & Exhibition, New Orleans, LA, Sep 25−28, 1994; SPE Paper #28505.

(12) Hammami, A.; Raines, M. A. Paraffin Deposition from Crude Oils: Comparison of Laboratory Results with Field Data. *Soc. Pet. Eng. J.* **1999**, *4*, 9.

(13) Meray, V. R.; Volle, J. L.; Schranz, C. J. P.; Le Marechal, P.; Behar, E. Influence of Light Ends on the Onset Crystallization Temperature of Waxy Crudes within the Frame of Multiphase Transport. Presented at the SPE Annual Technical Conference & Exhibition, Houston, TX, Oct 3−6, 1993; SPE Paper #26540.

(14) Misra, S.; Baruah, S.; Singh, K. Paraffin Problems in Crude Oil Production and Transportation: A Review. *SPE Prod. Facil.* **1995**, *10*, 50.

(15) Monger-McClure, T. G.; Tackett, J. E.; Merrill, L. S. Comparisons of Cloud Point Measurement and Paraffin Prediction Methods. *SPE Prod. Facil.* **1999**, *14*, 4.

(16) Patton, C. C.; Casad, B. M. Paraffin Deposition from Refined Wax−Solvent Systems. *Soc. Pet. Eng. J.* **1970**, *10* (1), 17.

(17) Singh, P.; Venkatesan, R.; Fogler, H. S.; Nagarajan, N. Morphological Evolution of Thick Wax Deposits during Aging. *AIChE J.* **2001**, *47*, 6.

(18) Weingarten, J. S.; Euchner, J. A. Methods for Predicting Wax Precipitation and Deposition. Presented at the SPE Annual Technical Conference & Exhibition, New Orleans, LA, Oct 5−8, 1986; SPE Paper #15654.

(19) Cawkwell, M. G.; Charles, M. E. Start-up of Pipelines Containing Gelled Crude Oils: Comparison of Improved Model and Pilot Pipeline Data. *J. Pipelines* **1989**, *7* (3), 265.

(20) Chang, C.; Boger, D. V.; Nguyen, Q. D. Influence of Thermal History on the Waxy Structure of Statically Cooled Waxy Crude Oil. *Soc. Pet. Eng. J.* **2000**, *5* (2), 148.

(21) Agrawal, K. M.; Khan, H. U.; Surianarayanan, M.; Joshi, G. C. Wax Deposition of Bombay High Crude Oil under Flowing Conditions. *Fuel* **1990**, *69*, 794.

(22) Cole, R. J.; Jessen, F. W. Paraffin Deposition. *Oil Gas J.* **1960**, *58* (38), 87.

(23) Bott, T. R. *Fouling of Heat Exchangers*; Elsevier: New York, 1995; pp 127−133, 141−147.

(24) Khan, H. U.; Dilawar, S. V. K.; Nautiyal, S. P.; Madhwal, D. C. Influence of *n*-Alkanes on the Cold Flow Properties of Their Solution in Different Solvent Systems. *Fuel* **1995**, *74*, 704.

(25) Mehrotra, A. K. Comments on: Influence of *n*-Alkanes on the Cold Flow Properties of Their Solution in Different Solvent Systems. *Fuel* **1996**, *75*, 246.

(26) Mehrotra, A. K. Comments on: Wax Deposition of Bombay High Crude Oil under Flowing Conditions. *Fuel* **1990**, *69*, 1575.

(27) Ghedamu, M.; Watkinson, A. P.; Epstein, N. Mitigation of Wax Buildup on Cooled Surfaces. In *Fouling Mitigation of Industrial Heat-Exchange Equipment*; Panchal, C. B., Bott, T. R., Somerscales, E. F. C., Toyama, S., Eds.; Begell House: New York 1997; pp 473−489.

(28) Bott, T. R.; Gudmunsson, J. S. Deposition of Paraffin Wax from Kerosene in Cooled Heat Exchanger Tubes. *Can. J. Chem. Eng.* **1977**, *55*, 381.

(29) Tiwary, D. Rheology and Phase Behavior of Highly Paraffinic Waxy Mixtures. M.Sc. Thesis, University of Calgary, Calgary, Canada, 2002.

(30) Cazaux, G.; Barre, L.; Brucy, F. Waxy Crude Cold Start: Assessment Through Gel Structural Properties. Presented at the SPE Annual Technical Conference & Exhibition, New Orleans, LA, Sep 27−30, 1998; SPE Paper #49213.

(31) Karan, K.; Ratulowski, J.; German, P. Measurement of Waxy Crude Properties Using Novel Laboratory Techniques. Presented at tne SPE Annual Technical Conference & Exhibition, Dallas, TX, Oct 1−4, 2000; SPE Paper #62945.

(32) Ronningsen, H. P.; Bjorndal, B.; Hansen, A. B.; Pedersen, W. B. Wax Precipitation from North Sea Crude Oils. 1. Crystallization and Dissolution Temperatures, and Newtonian and Non-Newtonian Flow Properties. *Energy Fuels* **1991**, *5*, 895.

(33) Bidmus, H. O. A Thermal Study of Wax Deposition from Paraffinic Mixtures. M.Sc. Thesis, University of Calgary, Calgary, Canada, 2003.

Received for review July 7, 2003
Revised manuscript received November 19, 2003
Accepted November 19, 2003

IE030573V